Pattern formation by spatially organized approximate majority reactions

Matthew R. Lakin[1] and Darko Stefanovic[1,2]

[1] Department of Computer Science, University of New Mexico, Albuquerque, NM, USA
[2] Center for Biomedical Engineering, University of New Mexico, Albuquerque, NM, USA

{mlakin,darko}@cs.unm.edu

Abstract. Pattern formation is a topic of great interest in biology and nanotechnology. In this paper we investigate a system of spatially-organized reactions inspired by a well-known distributed algorithm for approximate majority voting, and demonstrate that this system can lead to pattern formation from a randomly initialized starting state. We also show that the approximate majority reaction scheme can preserve an existing pattern in the face of noise, and that exerting control over reaction rates can influence the generated pattern. This work has potential applications in the rational design of pattern-forming systems in DNA nanotechnology and synthetic biology.

1 Introduction

Pattern formation is a fundamental topic in many areas of developmental biology. Turing [1] showed that certain systems of reaction-diffusion equations may give rise to spatiotemporal patterns, which can account for certain features of plant morphogenesis. Since nature has repeatedly found programmed pattern formation to be a robust means of directing the development of biological structures, the implementation of synthetic biochemical systems with similar spatial behavior has been a key goal of molecular programming [2, 3].

Spatiotemporal patterning systems such as those discovered by Turing depend on a balance between diffusion timescales: short-range inhibition and long-range activation are required for pattern formation. This fact has made it challenging to engineer synthetic biological systems for programmed pattern formation, because suitable diffusible molecules must be chosen to set up the morphogen gradients. In this paper we investigate the formation and preservation of spatial patterns by purely local reaction rules, which could form the basis of simplified synthetic patterning systems. The reaction rules in question are the approximate majority reaction scheme of Angluin *et al.* [4], which were originally developed as a distributed voting algorithm but which we employ as a set of spatial reaction rules to enable pattern formation.

The remainder of this paper is structured as follows. We introduce the approximate majority reaction scheme in Section 2 and use it as the basis for a spatial reaction system in Section 3. We present the results of simulations of the spatial approximate majority system in Section 4 and conclude with a discussion in Section 5.

2 The approximate majority system

The approximate majority (AM) system was introduced by Angluin *et al.* [4] as a leaderless algorithm for rapidly converging to a consensus between distributed agents with limited computing power. In its simplest form, the AM system is a chemical reaction network comprising three species (A, B, and X) and three reactions:

$$A + B \rightarrow X + X \tag{1}$$

$$A + X \rightarrow A + A \tag{2}$$

$$B + X \rightarrow B + B \tag{3}$$

From an initial state consisting of just species A and B, the intent of the AM reaction system is to convert all of the individuals into whichever species was initially present in the majority. When an A and a B meet, they are each converted into an X by reaction (1). When an X subsequently encounters an A or a B, the X is converted into another copy of the species it encountered, by either reaction (2) or reaction (3). The original formulation of the AM system assumes that the system is dilute and well-mixed, and therefore obeys the laws of mass action chemical kinetics. In this situation, the intuition behind the AM algorithm is that when an X species is created, it will be more likely to subsequently encounter whichever of A and B is present in the majority. Hence it is more likely for the initial majority species to catalyze the conversion of the minority species into the majority than for the initial minority species to catalyze the conversion of the majority species into the minority.

Implementations of the AM system using DNA strand displacement reactions have been studied both theoretically [5, 6] and in the laboratory [7], and networks with similar dynamic behavior have been observed in the regulatory systems that govern the cell cycle [8]. Hence this system of chemical reactions is of theoretical and practical interest as an object of study.

3 Spatially-organized approximate majority reactions

In this paper we consider the AM reactions in the context of a spatially-organized reaction system. To our knowledge, this is the first paper to consider the approximate majority system in a spatial context. As shown in Figure 1, we consider a grid of hexagonal cells in which every cell is labeled with a species: either A, B, or X. If two neighbouring cells are labeled with species that are *reactants* for one of the AM reactions from Section 2, then those cells can be relabeled with the *products* from the corresponding reaction, as shown in Figure 1. Our scheme is essentially a hexagonal cellular automaton—we choose to work in a hexagonal structure to avoid the potentially thorny issue of whether a given cell should be able to interact with a diagonally adjacent cell. In the interest of simplicity, we do not consider diffusion, which is required for alternative models of pattern formation, such as Turing patterning.

The rationale behind the use of AM reactions for spatial pattern formation is as follows. When species A and B occur in proximity, reaction (1) converts them both into X. Then, depending on whether A or B is predominant in that part of the grid, the occurrences of X will be preferentially converted to either A or B by reaction (2) or (3).

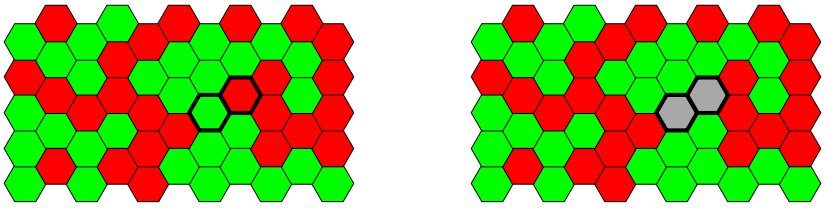

(a) A grid with two cells selected to interact (identified by a bold outline).

(b) The grid after relabeling the selected cells according to reaction (1).

Fig. 1: Hexagonal reaction grids with AM species and reactions. Here and henceforth, green cells represent species A, red cells represent species B, and grey cells represent species X.

By this mechanism, patterning in the occurrence of species A and B should be, roughly, preserved by the AM reactions. The AM reactions may also provide a means to generate a stable, spatially heterogeneous pattern from a uniformly-distributed, random starting state. Furthermore, if there is a possibility of noise that causes species A and B spontaneously to interconvert, the AM reactions may enable us to prevent a heterogeneous pattern from degenerating towards a uniform species distribution due to the effects of noise. Below we present the results of simulations designed to investigate these properties of the spatial AM reaction system.

4 Results

4.1 Pattern formation

We investigated the pattern formation capabilities of spatially organized AM reactions by running stochastic simulations starting from randomly-initialized, non-periodic grids, using a Gillespie-style algorithm [9]. In all simulations we used grids that are 40 cells wide and 40 rows tall. Each cell was initialized to either species A or B with equal probability—we did not include any cells of the intermediate species X in the initial grids. In these initial simulations, we fixed a uniform rate constant of 1.0 for all three AM reactions, throughout the grid. We ran all simulations for $100,000$ time units, as this was empirically found to be a suitable timescale to observe the phenomena under study.

The simulation algorithm can be summarized as follows. At the beginning of the simulation, the set of all possible reactions between cells in the initial grid was enumerated. The next reaction to occur was selected at random, with the probability of selecting a given reaction proportional to its rate constant. Simulation time was advanced by the time until the next reaction, which was drawn from an exponential distribution with mean $1/\rho$, with ρ being the rate constant of the selected reaction. The grid was transformed by applying the selected reaction, the select of possible reactions was updated to reflect the changes in the grid. The simulation loop was iterated until either the

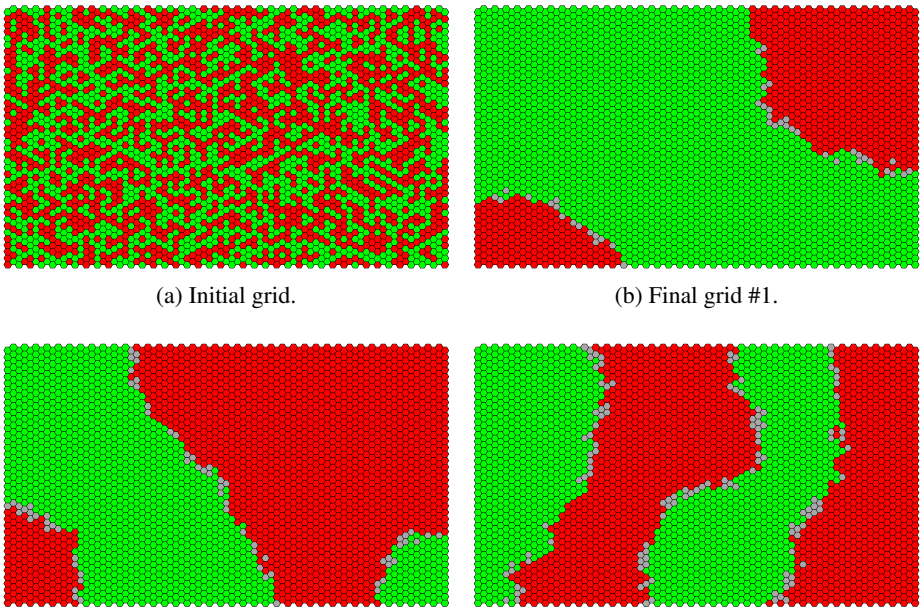

(a) Initial grid. (b) Final grid #1.

(c) Final grid #2. (d) Final grid #3.

Fig. 2: An initial grid and three example final grids generated from the initial grid via stochastic simulations.

time limit was reached or the grid reached a state from which no further reactions were possible.

Figure 2 shows a randomly-initialized grid together with three example grids derived from the initial grid by stochastic simulations using the AM reactions. In each case, we observe that the grid pattern evolves towards a state in which cells of a particular species accumulate into uniform patches, with the only subsequent reactions occurring at the borders between patches. These examples demonstrate that spatially-organized AM reactions can introduce long-distance order into a grid via purely localized reactions. This happens because the AM reactions allow the species that is dominant in a particular area of the grid to convert neighbouring cells of the other species to the dominant species, leading to the development of uniform patches.

To quantify this pattern-forming effect, we define a metric to measure the uniformity of the pattern around a given cell in a grid. We assume that each cell in the grid is labelled with a unique index i, and write $G(i)$ for the species of the cell in G that is labeled with i. We say that a *path*, p, is a finite list $[i_1,\ldots,i_n]$ of indices such that the grid cell labeled with i_{k+1} is a direct neighbour of the grid cell labeled with i_k and write $paths_G(i_1,i_2)$ for the set of paths that start from cell i_1 and end at cell i_2 in grid G. The *length*, $len(p)$, of a path p is the number of steps in the path, i.e., $len([i_1,\ldots,i_n]) = n-1$. For two indices $i_1 \neq i_2$ in the grid G, we write $dist_G(i_1,i_2)$ for the length of the shortest

path from i_1 to i_2 in grid G, i.e.:

$$dist_G(i_1, i_2) = \min(\{len(p) \mid p \in paths_G(i_1, i_2)\})$$

We write $sp_G(i_1, i_2)$ for the set of paths from $paths_G(i_1, i_2)$ that have length $dist_G(i_1, i_2)$. Then, we can define the n-neighbour metric, $\mu_{n,G}$, as follows:

$$\mu_{n,G}(i) = \{i' \mid dist_G(i, i') = n \wedge \exists p \in sp_G(i, i').\ \forall i'' \in p.\ G(i'') = G(i)\}$$

The set $\mu_{n,G}(i)$ contains the indices of all cells at distance n from i in the grid G that contain the same species as cell i and are connected to i by a path of length n that *only* traverses cells that also contain the same species as cell i. This set excludes cells that are either not part of the same contiguous patch as i or are in the same contiguous patch but not directly connected by a minimal-length path within the patch. This gives a robust measure of the uniformity of the pattern around cell i, because circuitous routes and non-connected cells are not counted. To account for the fact that cells near the edge of the grid may have fewer neighbours, in practice we report the size of $\mu_{n,G}(i)$ as a percentage of the total number of cells at distance n from i, i.e.:

$$\pi_{n,G}(i) = \left(\frac{|\mu_{n,G}(i)|}{|\{i' \mid dist_G(i, i') = n\}|} \right) \times 100$$

If $\pi_{n,G}(i)$ is close to 100% then the region of radius n around cell i has a highly uniform pattern containing the same species as i. If $\pi_{n,G}(i)$ is close to 0% then the pattern in the region of radius n around cell i is either highly fragmented or dominated by a different species than the species in i. The distribution of the values of $\pi_{n,G}(i)$ for all of the cells in a grid allows us to visualize the extent to which the pattern has separated out into well-defined, uniform patches. Figure 3 shows a worked example of computing the value of this metric for an example grid.

To measure the changes between grids G_1 and G_2 of the same size and shape, we use the Hamming distance, $H(G_1, G_2)$, which is the number of cells that have different species in G_1 and G_2. Since the grids have the same size, this can be straightforwardly expressed as a percentage of the total number of cells in the grid, which we write as $H_p(G_1, G_2)$.

We ran simulations starting from 200 randomly-initialized grids, with 50 stochastic runs from each initial grid. Figure 4a plots the percentage Hamming distance between the grid states at time t and $1,000$ time units earlier, i.e., $H_p(G(t), G(t-1000))$. The mean value of this metric decreases towards zero over time, showing that the rate of change of the pattern slows over time. Figure 4b quantifies the change in structure of the grid patterns by plotting the aggregated values of the $\pi_{3,G}$ metric for each cell in the initial and final grids from all $10,000$ grid simulations. Here and henceforth, we report the values of neighbour metrics for $n = 3$ because the metric computation masks features of size less than n, so for larger values of n we may fail to detect some pattern features. Conversely, for smaller values of n the metric may be overly sensitive to small-scale pattern features in the computation. The initial grids show a broad distribution of $\pi_{3,G}$ values between 0% and 40%, which corresponds to a chaotic initial pattern. Conversely, the vast majority of the final grid cells have $\pi_{3,G}$ values between 95% and

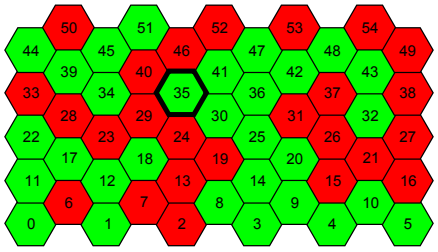

$\mu_{3,G}(35) = \{14, 20, 42\}$.

$|\{i' \mid dist_G(35, i') = 3\}| = 13$.

Hence, $\pi_{3,G}(35) = \frac{3}{13} \times 100 \approx 23\%$.

Fig. 3: Computing the value of the $\pi_{3,G}$ metric for cell 35 (identified by a bold outline) in an example grid. Note that $12, 17, 39 \notin \mu_{3,G}(35)$ because those cells are not connected to cell 35 by any path of cells with the same species as cell 35, i.e., species A. Furthermore, note that $8 \notin \mu_{3,G}(35)$ because it is not connected to cell 35 by a path of A cells with length 3 (the shortest such path is $[8, 14, 25, 30, 35]$, which has length 4).

100%, which means that almost all cells are surrounded by a highly homogeneous patch with a radius of at least 3 cells. Together, these results demonstrate that the grids tend to evolve towards a pattern consisting of homogeneous patches, where further interactions can only occur at patch boundaries, which causes the rate of change of the pattern to slow over time.

4.2 Pattern preservation in the face of noise

The ability of the spatial AM reaction scheme to generate patterns from randomized starting conditions should also make it well suited to preserve an existing pattern in the face of noise. To test this hypothesis, we augmented the standard AM reactions with two "noise" reactions that enable cells to unilaterally switch between species A and B with a noise rate ν, as follows:

$$A \xrightarrow{\nu} B \qquad\qquad B \xrightarrow{\nu} A.$$

Instead of starting from a grid with uniformly-distributed species, we generated a uniform grid of A cells and added a number of hexagonal patches of B cells at random positions and with random sizes. We fixed the rates of the standard AM reactions at 1.0, and ran a total of $1,000$ simulations (50 repetitions from 20 initial grids) to observe how well the spatial AM reactions preserved the initial pattern over $100,000$ time units in the face of noise reactions with rate $\nu = 0.1$. Example initial and final grids from these simulations are presented in Figure 5, where we see that noise reactions alone completely obliterate the initial pattern. However, the inclusion of AM reactions preserves the pattern as well (or better) than in the noise-free case where only AM reactions may occur. This may be explained by the observation that, when noise reactions are included, some time is spent suppressing noise instead of altering the overall grid pattern, meaning that the overall pattern may be modified less in a given period of simulation time.

Figure 6a plots the percentage Hamming distance between the grid state at time t and the initial grid state, i.e., $H_p(G(t), G(0))$. With just noise reactions, the mean value

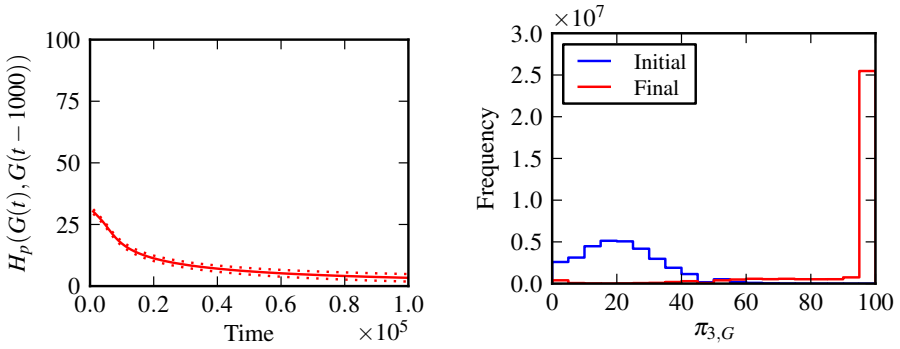

(a) Percentage Hamming distance between grid at time t and grid at time $t-1000$.

(b) Histograms of values of $\pi_{3,G}$ for all cells in all initial and final grids.

Fig. 4: Statistics from simulations with randomly-initialized grids. (a) Solid line is the mean from 10,000 simulations, and dotted lines are one standard deviation above and below the mean. (b) Values of $\pi_{3,G}$ were computed for all cells in the initial and final grids of 10,000 simulations and combined into two histograms.

of this metric converges to 50%, which is to be expected because the end result in this case will be a grid in which species A and B are uniformly distributed across the grid, so each cell has a 50% chance of being in a different species than in the initial grid. With both noise and AM reactions, however, the mean value rises more slowly. With just AM reactions, the mean value is in between the two, but with a larger variance due to the wide range of possible final states of the AM system. Figure 6b plots the distribution of $\pi_{3,G}$ values across all initial grids and final grids. In the initial grids, we see that almost all cells have $\pi_{3,G}$ values close to 100%, representing the highly ordered initial grid states. With just AM reactions, the final grid state is even more ordered, with an even higher percentage of cells whose $\pi_{3,G}$ values are close to 100%. With just noise reactions, the distribution in the final states is shifted significantly, such that almost all $\pi_{3,G}$ values are between 0% and 50%, which represents the expected highly fragmented pattern. With the inclusion of AM reactions, however, the final states retain a significant proportion of cells with $\pi_{3,G}$ values between 50% and 100%, with the highest frequency between 90% and 95%. There is an additional peak between 0% and 5% which we interpret as cells whose species have been flipped by noise but which have not yet been flipped back by the AM reactions. These results demonstrate that the AM reactions significantly slow pattern degradation by noise and help to preserve regions of homogeneity in the initial pattern. As simulation time tends to infinity, we expect that the combination of noise and AM reactions would eventually disrupt the initial pattern, but this process should be slowed by the AM reactions.

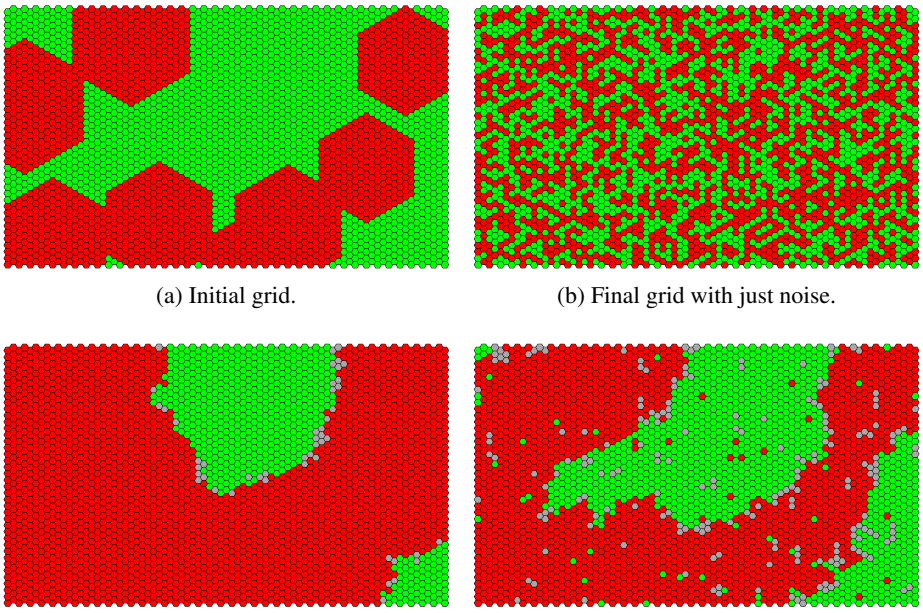

(a) Initial grid.

(b) Final grid with just noise.

(c) Final grid with just AM reactions.

(d) Final grid with noise *and* AM reactions.

Fig. 5: An initial grid and final grids generated under different reaction schemes from the initial grid via stochastic simulations. The noise rate was $\nu = 0.1$ in all cases.

4.3 Controlling pattern formation

In the reactions studied in Section 4.1, we observed pattern formation but without a means of controlling or predicting the resulting pattern. To demonstrate some control over the resulting pattern, we ran simulations starting from randomized initial grids with non-uniform reaction rates across the grid. We set the rate of the reaction $B+X \to B+B$ to $\rho < 1.0$ when one or both reactants are on the left-hand side of the grid (defined by a vertical line between the 20^{th} and 21^{st} columns of cells, which splits the grid into halves) and 1.0 when both reactants are on the right-hand side. The positions of the two reactants relative to each other were not used when computing these rates, only their absolute position on the grid. Similarly, we set the rate of the reaction $A+X \to A+A$ to be 1.0 when one or both reactants are on the left-hand side of the grid and $\rho < 1.0$ when both reactants are on the right-hand side. The rate of the reaction $A+B \to X+X$ was fixed at 1.0 across the whole grid. Since the reaction to replace X with B will be slower than the other reactions on the left-hand side of the grid, and the reaction to replace X with A will be slower than the other reactions on the right-hand side of the grid, the expected result of the simulations would be to generate a pattern in which the left-hand side of the grid is dominated by species A and the right-hand side of the grid is dominated by species B.

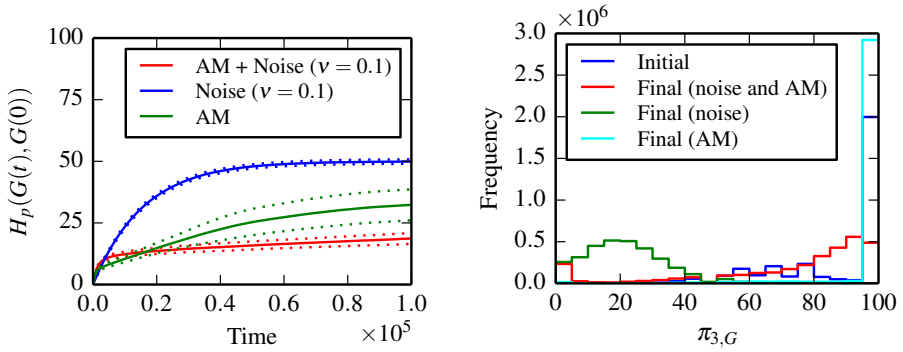

(a) Percentage Hamming distance between grid at time t and initial grid.

(b) Histograms of $\pi_{3,G}$ for all cells in all initial and final grids.

Fig. 6: Statistics from noise simulations. (a) Central lines are the mean from $1,000$ simulations, and dotted lines are one standard deviation above and below the mean. (b) Combined values of $\pi_{3,G}$ for all cells in the initial grids for $1,000$ simulations, and for the final grids in the presence of just AM reactions, just noise, and both noise and AM reactions. The noise rate was $\nu = 0.1$ in all cases.

We ran a total of $1,000$ simulations (50 repetitions from 20 initial grids, initialized with a uniform distribution of A and B) with non-uniform reaction rates as described above, using $\rho = 0.9$ as the slower reaction rate. Figure 7 shows an initial grid and example grids derived from it by a single stochastic simulation, at various time points. We observe that the grid pattern gradually moves from the chaotic initial grid towards a state in which the grid is split in half, with the left-hand side dominated by species A and the right-hand side dominated by species B. This supports our hypothesis that modifying the reaction rates as described above would produce a pattern of this kind.

Figure 8a plots the percentage Hamming distance between the grid state at time t and the expected grid G_{AB} (split exactly in half with the left-hand side containing only species A and the right-hand side containing only species B), i.e., $H_p(G(t), G_{AB})$. The mean value of this metric is initially around 50% due to the uniform initial distribution of species in the grid, rises as cells are initially converted to the intermediate X species, and subsequently decreases towards zero, indicating that the simulations are tending to converge towards the expected pattern. Figure 8b plots the distribution of $\pi_{3,G}$ values across all initial grids and final grids. As discussed above, the distributions are indicative of a chaotic initial state and a well-ordered final state with well-defined patches. These results show that increasing the relative rate of the reaction that converts X into a given species in one part of the grid biases the pattern towards that species in that area, demonstrating that we can control pattern formation by controlling reaction rates.

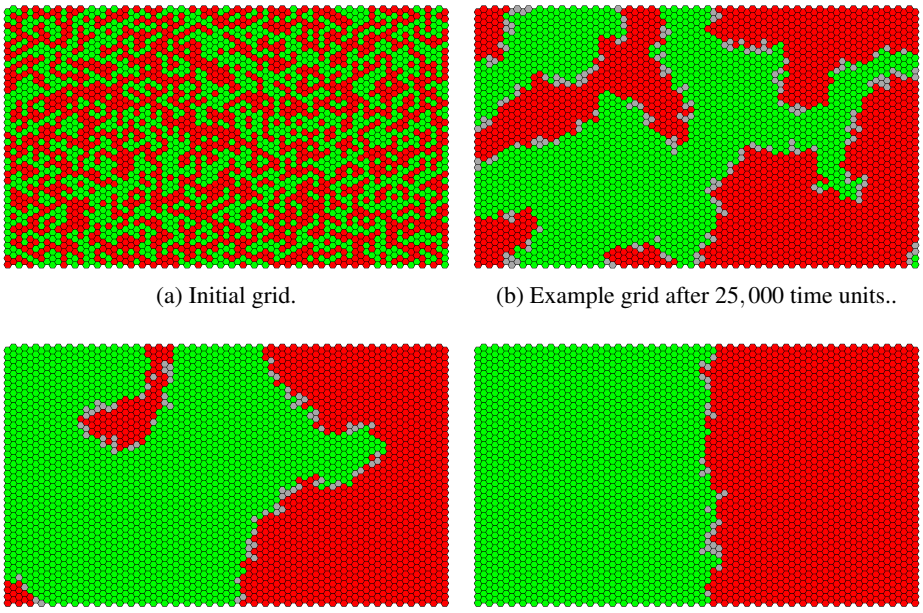

(a) Initial grid.

(b) Example grid after 25,000 time units..

(c) Example grid after 50,000 time units.

(d) Example grid after 75,000 time units.

Fig. 7: An initial grid and example grids generated by a stochastic simulation using non-uniform reaction rates to control pattern formation, with $\rho = 0.9$. The choice of reaction rates causes the chaotic initial pattern to move towards a pattern in which the left and right sides of the grid are dominated by species A and B, respectively.

5 Discussion

To summarize, we have demonstrated that the AM reaction scheme of Angluin *et al.* [4] provides a simple means for large-scale pattern generation via local interaction rules. The reactions enable the emergence of long-range order from random initial conditions and can preserve an established pattern in the face of noise. Manipulating reaction rates provides a possible means of controlling the generated pattern. This work has potential applications in morphogenetic engineering for synthetic biology [10], and in autonomous generation of patterned surfaces for DNA-templated nanofabrication [11].

Pattern formation is a well-developed field of study in many areas of science [12]. In statistical physics, a particular emphasis is placed on Ising spin models [13], which are capable of pattern generation [14]. In biology, reaction-diffusion systems were proposed by Turing [1] as the basis for various naturally-occurring patterns [15], and were first observed by Castets *et al.* [16]. Spatiotemporal patterns of predator and prey species are well-known in ecology, most famously predicted by the Lotka-Volterra model [17, 18]. Pattern formation in chemistry is known to occur in a number of systems, in particular the Belousov-Zhabotinsky reaction [19, 20], which can exhibit non-trivial spatiotem-

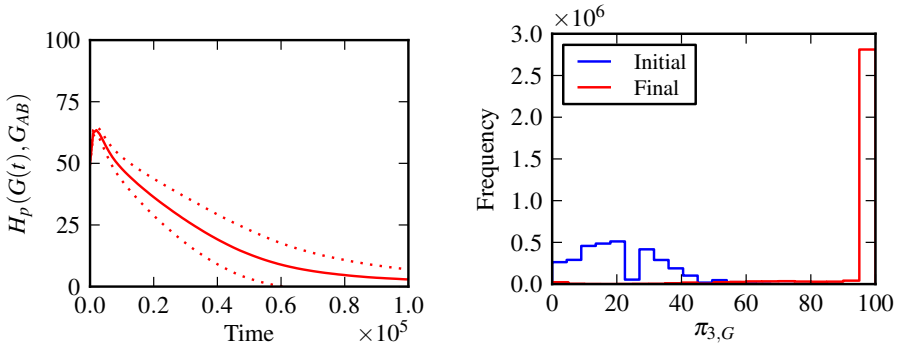

(a) Percentage Hamming distance between grid at time t and expected grid.

(b) Histograms of $\pi_{3,G}$ for all cells in all initial and final grids.

Fig. 8: Statistics from simulations to control pattern formation. (a) The expected grid is split in half, with the left-hand side containing only species A and the right-hand side containing only species B. Solid line is the mean from $1,000$ simulations and dotted lines are one standard deviation above and below the mean. (b) Values of $\pi_{3,G}$ were computed for all cells in the initial grids for $1,000$ simulations, and for the final grids obtained via stochastic simulations, using non-uniform reactions with $\rho = 0.9$.

poral behaviour [21, 22]. In DNA nanotechnology, similar spatiotemporal waves have been observed in synthetic genetic oscillators [3]. To our knowledge, the pattern formation scheme proposed in this paper is novel in that it specifically exploits the properties of the AM reactions as a rationally designed method to impose spatial order via local communication, as opposed to long-range coordination. Our work has clear links to recent attempts to understand the role of the AM reaction scheme in cell biology [8] and to implement the AM reactions in mass action chemistry using two-domain DNA strand displacement [7].

For future work, it will be important to investigate the robustness of the pattern formation process to changes in the experimental conditions. Our results from Section 4.3 suggest that variations in reaction rates can have dramatic effects on the generated pattern, which may be challenging for a practical implementation. It will also be interesting to investigate other methods of exerting control over the resulting pattern, and the classes of patterns that can be formed or preserved by this mechanism, e.g., patterns with complicated shapes such as mazes with thin walls of species A overlaid on a background of species B. As an alternative to modulating reaction rates, it may be possible to augment the basic AM reaction set with additional reactions to favour certain kinds of pattern. A detailed theoretical study of this pattern formation mechanism, e.g., to prove properties of the way the patterns evolve over time, may shed light on these issues. In particular, incorporating a temperature parameter and expressing reaction rates as functions of temperature may reveal non-linear, temperature-dependent effects in the

pattern formation process. It may also be enlightening to simulate spatial AM reactions on larger grids, and in a toroidal cellular automaton framework with periodic boundary conditions. These would reduce any edge effects, as discussed in Section 4.1.

From a practical perspective, spatial reaction grids such as those described in this paper could be constructed in the laboratory using hexagonal DNA origami assembled on a pre-formed scaffold [23] or on tethered microspheres [24, 25]. The pattern-generating interactions could be implemented using DNA strand displacement reactions [26, 7]. Alternatively, spatial AM reaction systems could be constructed within networks of communicating bacteria [27–30], providing a means for rationally designed pattern generation [31, 32] via local interactions, without a reliance on long-range diffusion.

Acknowledgments

This material is based upon work supported by the National Science Foundation under grants 1028238 and 1318833. M.R.L. gratefully acknowledges support from the New Mexico Cancer Nanoscience and Microsystems Training Center.

References

1. A. M. Turing. The chemical basis of morphogenesis. *Philosophical Transactions of the Royal Society B*, 237(641):37–72, 1952.
2. S. M. Chirieleison, P. B. Allen, Z. B. Simpson, A. D. Ellington, and X. Chen. Pattern transformation with DNA circuits. *Nature Chemistry*, 5:1000–1005, 2013.
3. A. Padirac, T. Fujii, A. Estévez-Torres, and Y. Rondelez. Spatial waves in synthetic biochemical networks. *Journal of the American Chemical Society*, 135(39):14586–14592, 2013.
4. D. Angluin, J. Aspnes, and D. Eisenstat. A simple population protocol for fast robust approximate majority. *Distributed Computing*, 21(2):87–102, 2008.
5. M. R. Lakin, D. Parker, L. Cardelli, M. Kwiatkowska, and A. Phillips. Design and analysis of DNA strand displacement devices using probabilistic model checking. *Journal of the Royal Society Interface*, 9(72):1470–1485, 2012.
6. M. R. Lakin, A. Phillips, and D. Stefanovic. Modular verification of DNA strand displacement networks via serializability analysis. In D. Soloveichik and B. Yurke, editors, *Proceedings of the 19th International Conference on DNA Computing and Molecular Programming*, volume 8141 of *Lecture Notes in Computer Science*, pages 133–146. Springer-Verlag, 2013.
7. Y.-J. Chen, N. Dalchau, N. Srinivas, A. Phillips, L. Cardelli, D. Soloveichik, and G. Seelig. Programmable chemical controllers made from DNA. *Nature Nanotechnology*, 8:755–762, 2013.
8. L. Cardelli and Attila Csikász-Nagy. The cell cycle switch computes approximate majority. *Scientific Reports*, 2:656, 2012.
9. D. T. Gillespie. Exact stochastic simulation of coupled chemical reactions. *Journal of Physical Chemistry*, 81(25):2340–2361, 1977.
10. R. Doursat, H. Sayama, and O. Michel. A review of morphogenetic engineering. *Natural Computing*, 12(4):517–535, 2013.
11. H. Li, J. D. Carter, and T. H. LaBean. Nanofabrication by DNA self-assembly. *Materials Today*, 12(5):24–32, 2009.

12. M. C. Cross and P. C. Hohenberg. Pattern formation outside of equilibrium. *Reviews of Modern Physics*, 65(3):851–1112, 1993.
13. E. Ising. Beitrag zur Theorie des Ferromagnetismus. *Zeitschrift für Physik*, 31(1):253–258, 1925.
14. T. Antal, M. Droz, J. Magnin, A. Pekalski, and Z. Rácz. Formation of Liesegang patterns: Simulations using a kinetic Ising model. *Journal of Chemical Physics*, 114(8):3770–3775, 2001.
15. J. D. Murray. A pre-pattern formation mechanism for animal coat markings. *Journal of Theoretical Biology*, 88:161–199, 1981.
16. V. Castets, E. Dulos, J. Boissonade, and P. De Kepper. Experimental evidence of a sustained standing Turing-type nonequilibrium chemical pattern. *Physical Review Letters*, 64:2953–2956, 1990.
17. A. J. Lotka. Undamped oscillations derived from the law of mass action. *Journal of the American Chemical Society*, 42:1595–1599, 1920.
18. V. Volterra. Fluctuations in the abundance of a species considered mathematically. *Nature*, 118:558–560, 1926.
19. H. Degn. Oscillating chemical reactions in homogeneous phase. *Journal of Chemical Education*, 49:302–307, 1972.
20. A. T. Winfree. Spiral waves of chemical activity. *Science*, 175:634–635, 1972.
21. R. J. Field and R. M. Noyes. Explanation of spatial band propagation in the Belousov reaction. *Nature (London)*, 237:390–392, 1972.
22. A. T. Winfree. Varieties of spiral wave behaviour: an experimentalist's approach to the theory of excitable media. *Chaos*, 1:303–334, 1991.
23. Z. Zhao, Y. Liu, and H. Yan. Organizing DNA origami tiles into larger structures using preformed scaffold frames. *Nano Letters*, 11:2997–3002, 2011.
24. B. M. Frezza, S. L. Cockroft, and M. R. Ghadiri. Modular multi-level circuits from immobilized DNA-based logic gates. *Journal of the American Chemical Society*, 129:14875–14879, 2007.
25. R. Yashin, S. Rudchenko, and M. Stojanovic. Networking particles over distance using oligonucleotide-based devices. *Journal of the American Chemical Society*, 129:15581–15584, 2007.
26. D. Y. Zhang and G. Seelig. Dynamic DNA nanotechnology using strand-displacement reactions. *Nature Chemistry*, 3(2):103–113, Feb 2011.
27. M. Weitz, A. Mückl, K. Kapsner, R. Berg, A. Meyer, and F. C. Simmel. Communication and computation by bacteria compartmentalized within microemulsion droplets. *Journal of the American Chemical Society*, 136(1):72–75, 2014.
28. R. Silva-Rocha and V. de Lorenzo. Engineering multicellular logic in bacteria with metabolic wires. *ACS Synthetic Biology*, 2013.
29. W. Bacchus, M. Lang, M. D. El-Baba, W. Weber, J. Stelling, and M. Fussenegger. Synthetic two-way communication between mammalian cells. *Nature Biotechnology*, 30(10):991–998, 2012.
30. T. Danino, O. Mondragón-Palomino, L. Tsimring, and J. Hasty. A synchronized quorum of genetic clocks. *Nature*, 463:326–330, 2010.
31. T. J. Rudge, P. J. Steiner, A. Phillips, and J. Haseloff. Computational modeling of synthetic microbial biofilms. *ACS Synthetic Biology*, 1:345–352, 2012.
32. N. Dalchau, M. J. Smith, S. Martin, J. R. Brown, S. Emmott, and A. Phillips. Towards the rational design of synthetic cells with prescribed population dynamics. *Journal of the Royal Society Interface*, 9(76):2883–2898, 2012.